

Laser cooling and launching performance in a (1,1,1)-geometry atomic fountain

E.A. Donley, T.P. Heavner, J. W. O'Brien and

S.R. Jefferts

NIST Time and Frequency Division
325 Broadway, Boulder, CO 80305
edonley@boulder.nist.gov

F.Levi

Istituto Elettrotecnico Nazionale "G. Ferraris",
Str. Delle Cacce 91,
Torino, Italy

Abstract— We have successfully cooled and launched cesium atoms in the (1,1,1) atomic fountain geometry at temperatures as low as 0.8 μK . This corresponds to a root-mean-square thermal velocity of 0.7 cm/s, which is two times the photon recoil velocity of 0.35 cm/s. Factors that limit the final temperature are presented in detail.

I. INTRODUCTION

In order to optimize the parameters to obtain the lowest uncertainty for the spin-exchange frequency shift, the atom throughput in an atomic fountain must be maximized. By atom throughput, we mean the number of atoms that emerge from the Ramsey cavity on the way down divided by the number of atoms that enter the cavity on the way up. When the atom throughput is low, some atoms that contribute to the spin-exchange shift do not contribute to the return atom signal and the clock stability. The atom throughput in an atomic fountain is a complicated function of many parameters, including the initial size of the atom ball, the size of the aperture in the Ramsey cavity, the cavity's height, and the root-mean-square (RMS) atom thermal velocity, v_{RMS} .

The atomic fountain NIST-F2 that is under development will operate in the (1,1,1) atomic fountain geometry as opposed to the more traditional (0,0,1) geometry that we use for NIST-F1 [1]. In the (1,1,1) geometry, the beam orientation is such that there are 3 upward-traveling beams and 3 downward-traveling beams, all of which make an angle of $\pm 35.3^\circ$ with the horizontal plane. Ultimately, we would like to be able to launch more than one atom ball per clock cycle in order to be able to run at lower density to reduce the uncertainty of the spin-exchange shift [2]. In contrast to the (0,0,1) geometry, in the (1,1,1) geometry none of the molasses beams travel along the flight tube where they would interfere with launching multiple atom balls per clock cycle.

In terms of the temperature, the RMS atom velocity is $v_{RMS} = \sqrt{k_B \cdot T / m}$, where m is the mass of a cesium atom and k_B is Boltzmann's constant. Throughout the paper we usually refer to effects on v_{RMS} when we evaluate the laser

cooling sensitivities rather than the effects on the temperature. The photon recoil velocity, v_{recoil} , sets the scale for the velocities that we are investigating since we are cooling the atoms down to velocities that correspond to a few times v_{recoil} . Therefore it is convenient to characterize v_{RMS} and changes in v_{RMS} in terms of a corresponding number of photon recoils. The recoil velocity is $v_{recoil} = h / (\lambda \cdot m)$, where h is Plank's constant, λ is the wavelength of the transition, and m is the atomic mass. For the D2 transition in ^{133}Cs , $v_{recoil} = 0.35 \text{ cm/s}$.

Before we committed to a final design for the collection and launch chamber of NIST-F2 we wanted to learn what factors would limit the temperature, and also to see how cold we could get the atoms. So far, we have been able to cool and launch cesium atoms at temperatures as low as 0.8 μK . This corresponds to a RMS thermal velocity $v_{RMS} = 0.7 \text{ cm/s}$, which is twice the photon recoil velocity of 0.35 cm/s. The achieved thermal velocity is 30 % lower than the 1 cm/s value that we reported last year [3], but it is still 25 % larger than what we achieve in NIST-F1. We are hopeful that the studies of the sensitivities that we have performed with our prototype apparatus have enabled us to design a vacuum chamber for NIST-F2 with which we can achieve yet lower atom temperatures.

This paper is organized as follows. In section II we present details of the apparatus and experimental procedures. In section III we discuss specific sensitivities of the achievable atom temperature to several parameters, and in section IV we present design details for the NIST-F2 atom collection and launch chamber and the status of its construction.

II. APPARATUS AND EXPERIMENTAL PROCEDURE

Figure 1 is a picture of the apparatus. The beams for the optical molasses are supplied via polarization-maintaining fibers to laser beam collimators that are bolted directly to the vacuum flanges on the apparatus. In our initial experiments we tried a nonadjustable collimator design. The vacuum chamber for the atom collection region was machined such

that the cube faces are orthogonal to the molasses beam axes, so we initially tried locating the laser beam collimators orthogonal to the beam faces. We discovered that the collimator mounts still had to be shimmed to be able to optimize the signal amplitude and minimize the atom temperature. The alignment procedure was tedious, and we were unsure if the true optimum was reached.

For the results presented here, we used new collimator mounts that allow us to smoothly adjust the angular alignment of the molasses beams by ~ 10 mrad in two orthogonal directions. The design of the mounts is such that the angular alignment can be varied without changing the position at which the beams cross in the molasses region. These adjustable collimators have made the experiment much easier to optimize.

The laser power for each of the six molasses beams was independently servoed by controlling the RF power applied to six double-pass acousto-optic modulators (AOMs) with voltage-controlled attenuators. The design required having an independent double-pass AOM [4] for each of the six molasses beams. The set-point voltage for the servos was computer-generated and was the same for all six servos. The intensity ramp for the postcool was programmed into the set-point voltage and the servos remained locked during the postcool. With the servo system locked the signal amplitude would remain constant for days at a time, which has simplified optimization and improved the stability of the apparatus.



Figure 1. The apparatus.

Each laser beam collimator had a polarizer followed by a beam sampler after the fiber jack output. The beam sampler directed $\sim 1\%$ of the light to a photodiode. The photodiode output was amplified and fed into a voltage summing circuit along with an adjustable offset voltage. This offset allowed us to account for small deviations in the background levels. The feedback resistance of the summing circuit was also adjustable to account for gain variations in the photodiode amplifiers. During the various experiments in the optimization process, the laser power per beam varied from I_{sat} to $10 \cdot I_{sat}$, depending on the molasses beam size. The beam diameter varied from 8 mm to 21 mm (FW 1/e²), depending on the experiment.

We noted in [3] that we could observe the lowest atom temperature by allowing the atoms to fall for ~ 25 ms before launching them, which could be explained because of better overlap between the atom ball and the molasses beams during the postcool [5]. Dropping the atoms also increases the number of atoms launched. It is possible to accomplish the same increase in number of atoms launched in only a few milliseconds by shifting the molasses beam frequencies to push the atoms downward instead of simply dropping them. It also turns out that we achieve the highest number of launched atoms, the highest return fraction, and the lowest thermal velocities when we “precool” the atoms before launch. The optimum laser frequency sequence that we found is shown in Figure 2a. The precool sequence consists of a sudden jump in frequency of 0.6 MHz (-0.6 MHz) for the down (up) beams followed by a -40 MHz linear frequency ramp for 2.3 ms. The frequency ramp cools the atoms in the moving frame before launch. Precooling the atoms increased the number of launched atoms by $\sim 10\%$ and reduced v_{RMS} by $\sim 0.15 \cdot v_{recoil}$.

The atoms were much less sensitive to the details of the intensity than to the frequency of the molasses beams during the postcool. The RMS velocity could typically be reduced by a few percent by tuning the postcool intensity ramp, whereas the RMS thermal velocity goes up by an order of magnitude when no postcool frequency ramp is applied. A typical postcool intensity sequence that minimized v_{RMS} is shown in Figure 2b. Other intensity ramps worked similarly, but the intensity ramps that were most effective turned down the beam intensity on a short time scale. In the example in Figure 2b, the intensity was turned down exponentially with a time constant of 180 μ s. We did not observe a dependence of the final RMS thermal velocity on initial molasses beam intensity.

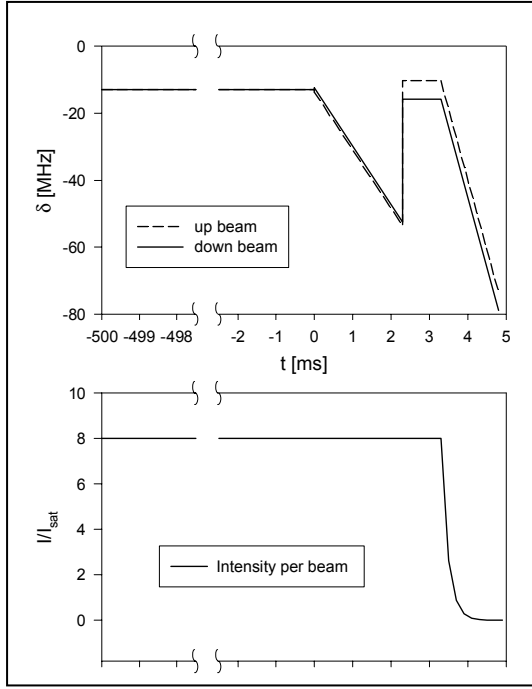


Figure 2. (a.) Typical launch frequency detunings for the up (dashed line) and down (solid line) beams. The origin of the time axis coincides with the start of the pre-cool stage. (b.) Laser beam intensity dependence. In this example, the intensities for the optical molasses stage were 8 times the saturation intensity. We used intensities between one and ten times I_{sat} .

To determine the thermal velocity of the launched atoms, the atom spatial distribution was measured in a detection light sheet 41 cm above the molasses region for balls of atoms both on their way up and on their way down. The atom velocity distribution was then found via one of two techniques. Either we applied a numerical deconvolution procedure and the rms velocity was assigned as the Gaussian width of the resulting velocity distribution, or we assumed Gaussian distributions for the initial ball size and velocity spread and modeled the ball size with the relation $\sigma^2(t) = \sigma_0^2 + v_{RMS}^2 t^2$, where σ_0 is the initial Gaussian ball size and $\sigma(t)$ is the Gaussian width of the ball of atoms as a function of time after launch. Using the Gaussian model worked better than the numerical deconvolution procedure for the lowest achieved thermal velocities, because for narrower distributions we could not low-pass filter the data as much without broadening the spatial distribution of the upward atom ball.

The lowest temperature that we have achieved thus far is 0.8 μK . The time-of-flight data for this measurement are shown in Figure 3. 0.8 μK corresponds to an atom thermal velocity of 0.7 cm/s, which is $2 \cdot v_{recoil}$. At 0.8 μK , Monte Carlo simulations of the atom throughput for NIST-F2 indicate that 56 % of the atoms entering a microwave cavity with apertures of 7 mm radius will return to the detection zone. This is a good atom throughput, but it is not quite as

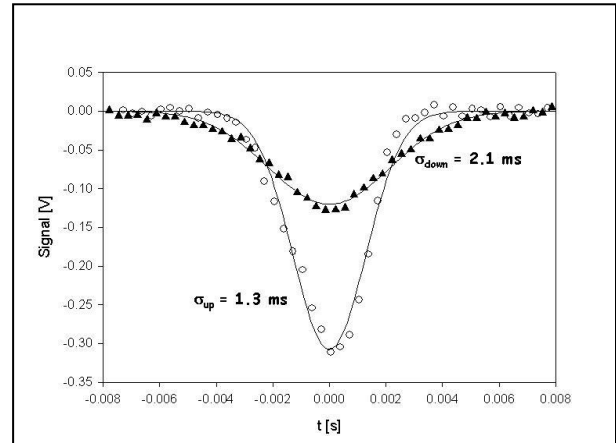


Figure 3. Time of flight data for the lowest achieved temperature for upward (\circ) and downward (\blacktriangle) travelling balls of atoms. The data have been shifted to be centered around $t = 0$ for presentation. The up and down curves have been fitted to Gaussians. Note that the detection beam intensity was turned down to $I_{sat}/20$, where I_{sat} is the saturation intensity. We used such a low intensity to minimize heating from scattered light. For this measurement, the atoms were launched to a height of 0.87 m, and the atom ball velocity was 3.01 m/s in the detection zone.

good as that achieved in NIST-F1, with which we achieve 0.5 μK , which corresponds to $1.5 \cdot v_{recoil}$ and an atom throughput of 66 %.

We observed a correlation between molasses beam diameter and RMS thermal velocity (discussed below), and our value of $v_{RMS} = 0.7$ cm/s was achieved with molasses beams of 8 mm in diameter (FW 1/e²). For 21 mm diameter beams, the lowest thermal velocity that we achieved was $v_{RMS} = 0.8$ cm/s.

III. SPECIFIC SENSITIVITIES

In the long run, we will need to use molasses beams that are as large as possible to minimize the atom density at a given signal-to-noise ratio, so we have studied the dependence of v_{RMS} on many parameters to try to learn how to achieve lower temperatures.

The parameter space for adjusting the (1,1,1) system is very large. We have tried combinations of many different parameters over the past year. In fact, we have changed so many different things that it is difficult to compare data collected today to data that was collected six months ago. Even where the data are difficult to compare, there are clearly some reproducible trends that indicate sensitivities to certain parameters. Here we summarize those trends.

A. Molasses beam quality and size

In trying different collimator lens combinations to achieve smooth, Gaussian beams, we observed a dependence of v_{RMS} on molasses beam size, with lower temperatures achieved for smaller molasses beams. With everything else held equal, in going from 8 to 21 mm beams of high-quality (FW 1/e^2), v_{RMS} increased from 0.7 to 0.8 cm/s. This corresponds to a RMS velocity increase of $\sim 0.3 \cdot v_{recoil}$, which would reduce the atom throughput by $\sim 10\%$. This might be related to magnetic-field issues, as discussed below in section IIIB.

The minimum achievable thermal velocity also depends on beam quality. In trying to produce large beams, all of the multi-lens combinations that we tried produced bright rings at the beam edges, and the light distribution clearly changed with distance from the collimator. The problems were the worst when we used lenses of short focal length close to the output of the fibers. We had the best beam quality when we used a single lens spaced a distance of one focal length from the fiber output.

We tried two different lens systems that produced beams of about the same size (2 cm FW 1/e²) but of different beam quality. One combination was a Galilean telescope with -30 and +75 mm lenses that produced beams with bright rings on the edges. The other collimator design had a single 200 mm achromat lens positioned one focal length from the output of the single-mode fiber. With the higher-quality beams achieved with the single achromat lens design, we observed a value v_{RMS} that was $0.14 \cdot v_{recoil}$ lower. A drawback to the single-lens design is that the collimators are then 50 % longer. While it makes sense that higher-quality beams give better results, it is not clear to us why smaller beams are more effective. A possible explanation is given in the next section.

B. Magnetic-field inhomogeneities

It is difficult to know for sure whether magnetic-field inhomogeneities limit the achievable temperature in our apparatus, because it is difficult to reduce any gradients that are present without major modifications to the apparatus. However, several pieces of evidence suggest that we are limited by magnetic-field gradients in the molasses chamber that limit the effectiveness of the postcool sequence.

Evidence that magnetic-field gradients can be a problem was revealed when we split the vertical Helmholtz coils to independently control their currents. We were then able to reduce v_{RMS} by $0.2 \cdot v_{recoil}$, which implies that there was an underlying field gradient that was reduced by splitting the coils and effectively using a sum of Helmholtz and anti-Helmholtz coils. The optimal currents for the top and bottom coils were 0.8 A for the upper coil and 0.3 A for the lower coil, which implies a magnetic-field gradient in the molasses region of 2 mG/mm given the coil geometry. Therefore variations in field on the order of 10 mG over the extent of

the molasses during collection and launch would not be out of the question.

Other evidence suggesting that we are limited by magnetic field inhomogeneity is that we achieve the lowest temperatures for the smallest molasses beams. A smaller optical molasses would not sample as large a variation in magnetic fields and may not be as limited by field inhomogeneities.

We also observed lower values of v_{RMS} when we launched atoms to a lower launch height. When launching to lower launch height, the atoms have a lower launch velocity and do not move as far before the end of the postcool sequence, and so they experience a smaller range of magnetic fields at launch.

When the magnetic field in an optical molasses is non-zero, Zeeman shifts can affect the temperature achievable with laser cooling [6]. Such a heating mechanism could possibly be at play here.

C. Scattered light

We observed heating by scattered light, particularly at the lowest atom velocities that we achieved. This heating occurred from two sources. One source of heating was from repump light tuned to the $F=3 \rightarrow F'=4$ transition that was absorbed by thermal atoms in the molasses region and scattered up the flight tube in resonance with the $F=4 \rightarrow F'$ transitions. The other source of heating was from scattered detection light when the detection beams were turned on long before the atoms arrived in the detection zone. Each source of heating increased v_{RMS} by $\sim 0.1 \cdot v_{recoil}$.

Both of these sources of heating were reduced by properly shuttering the beams. Also, scattered light from detection-beam optics has been reduced by design improvements. Our initial detection beam optical set-up was designed to be compact so that it could be contained inside the outermost layer of magnetic shielding. Light was fed to a cylindrical collimator through a polarization-maintaining fiber mounted to a plate in the back of a commercial lens tube. The lens tube was bolted directly to the detection beam entrance window. A drawback of the design was that the retroreflected detection beams scattered off the collimator optics at a position close to the vacuum-chamber windows. In the final NIST-F2 design we will mount the optics outside the magnetic shielding and cut holes through the shields so that the beams can enter the windows.

IV. NIST-F2 ATOM COLLECTION AND LAUNCH CHAMBER

The final version of the NIST-F2 atom collection and launch chamber is being built with special attention to minimizing stray magnetic fields. Figure 4 is a drawing of the apparatus. The holes in the vacuum chamber are being cut with electric-discharge machining techniques, which minimize work hardening and therefore the creating of regions of induced magnetization. Some milling will need to

be done, but the chamber will be annealed after the cuts have been made. Also, NIST-F2 will be mounted on a non-magnetic base instead of an ordinary soft-iron optical table as we have had for the measurements reported here.

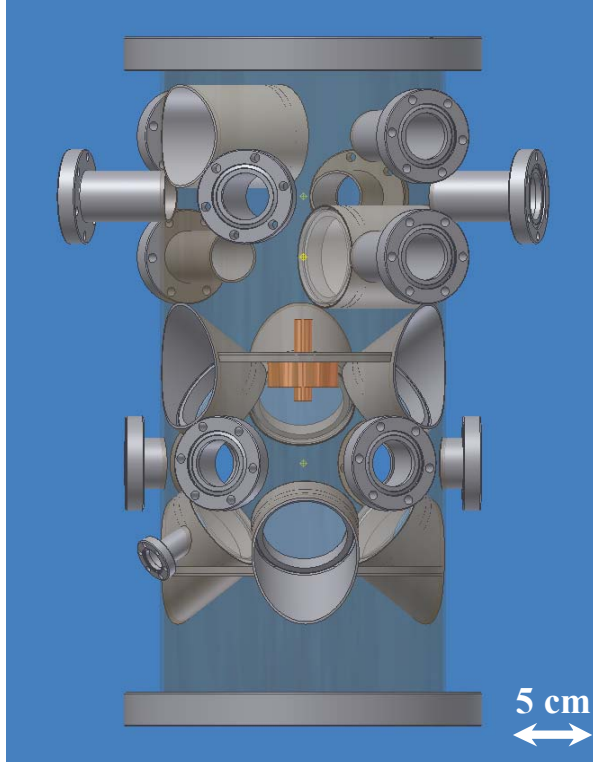


Figure 4. A drawing of the NIST-F2 atom launch and detection chamber. The outer wall of the vacuum chamber is shown as transparent in the figure for clarity. The chamber is constructed from a straight section of 304 stainless steel pipe that has a diameter of 203 mm and has 254 mm conflat flanges on the top and bottom. The lower half of the chamber will serve as the atom collection and launch region, while the upper half will be used for detection. The holes in the pipe are all cut with electric discharge machining techniques. Two plates welded into the interior of the pipe serve multiple purposes. Both plates help to locate the tubing for the (1,1,1) reentrant windows for welding them in place. In addition, the upper plate serves as a baffle for differential pumping and as a mounting plate for the state-selection cavity. There are multiple axes in the horizontal plane of the molasses chamber to be used for optical access and for eventually loading the molasses with a low-velocity intense-source of atoms [8]. A 34 mm conflat port at an angle of -30° from the molasses midplane can be used for loading atoms with a cesium oven. The total height of the chamber is ~53 cm.

The prototype apparatus that we have used to perform the measurements did not have microwave cavities or any other apertures along the toss tube. It is likely that we will measure lower temperatures for the interrogated atoms when we have apertures, because the atoms on the outer edges of the molasses may not have a postcool as effective as that for the atoms in the center of the molasses owing to the less optimal beam overlap during the postcool.

With these improvements, it is possible that we will be able to operate with larger optical molasses beams at a lower temperature than the 0.8 μK thus far achieved, and hopefully at the 0.5 μK level currently achieved in NIST-F1.

ACKNOWLEDGMENTS

The authors thank Mike Lombardi, Tom O'Brian, Tom Parker, Jon Shirley, David Smith, and Ying-Ju Wang for many valuable discussions and for valuable comments on this manuscript. This work is a contribution of NIST, an agency of the U.S. government, and is not subject to copyright.

REFERENCES

- [1] S.R. Jefferts et al., "Accuracy evaluation of NIST-F1," *Metrologia*, vol. 39, pp. 321-326, 2002.
- [2] F. Levi, A. Godone, and L. Lorini, "Reduction of the cold collisions frequency shift in a multiple velocity fountain: a new proposal," *IEEE Trans. Ultrason., Ferroelect., Freq. Contr.*, vol. 48, pp. 847-850, 2001.
- [3] E.A. Donley, T.P. Heavner, M.O. Tataw, F. Levi, and S.R. Jefferts, "Progress towards the second-generation atomic fountain clock at NIST," 2004 IEEE IFCS, Montréal, Canada August 2004, pp. 82.
- [4] E.A. Donley, T.P. Heavner, F. Levi, M.O. Tataw, and S.R. Jefferts, "Double-pass acousto-optic modulator system," *Rev. Sci. Instrum.* vol. 76, 063112, 2005.
- [5] W.M. Klipstein, unpublished.
- [6] S.Q. Shang, B. Sheehy, P. van der Straten, and H. Metcalf, "Velocity-selective magnetic-resonance laser cooling," *Phys. Rev. Lett.*, vol. 65, pp. 317-320, 1990.
- [7] Z.T. Lu, K.L. Corwin, M.J. Renn, M.H. Anderson, E.A. Cornell, and C.E. Wieman, "Low-velocity intense source of atoms from a magneto-optical trap," *Phys. Rev. Lett.*, vol. 77, pp. 3331-3334, 1996.
- [8] E.A. Donley, T.P. Heavner, and S.R. Jefferts, "Optical molasses loaded from a low-velocity intense source of atoms: an atom source for improved atomic fountains," *IEEE Trans. Instrum. Meas.*, accepted for publication.